Tensile Forces and Shape Entropy Explain Observed Crista Structure in Mitochondria

M. Ghochani,[†] J. D. Nulton,[‡] P. Salamon,[‡*] T. G. Frey,[§] A. Rabinovitch,[¶] and A. R. C. Baljon[†]
[†]Department of Physics, [‡]Department of Mathematical Sciences, and [§]Department of Biology, San Diego State University, San Diego, California; and [¶]Department of Physics, Ben-Gurion University of the Negev, Beer-Sheva, Israel

ABSTRACT We present a model from which the observed morphology of the inner mitochondrial membrane can be inferred as minimizing the system's free energy. In addition to the usual energetic terms for bending, surface area, and pressure difference, our free energy includes terms for tension that we hypothesize to be exerted by proteins and for an entropic contribution due to many dimensions worth of shapes available at a given energy. We also present measurements of the structural features of mitochondria in HeLa cells and mouse embryonic fibroblasts using three-dimensional electron tomography. Such tomograms reveal that the inner membrane self-assembles into a complex structure that contains both tubular and flat lamellar crista components. This structure, which contains one matrix compartment, is believed to be essential to the proper functioning of mitochondria as the powerhouse of the cell. Interpreting the measurements in terms of the model, we find that tensile forces of ~20 pN would stabilize a stress-induced coexistence of tubular and flat lamellar cristae phases. The model also predicts a pressure difference of -0.036 ± 0.004 atm (pressure higher in the matrix) and a surface tension equal to 0.09 ± 0.04 pN/nm.

INTRODUCTION

For many years, our view of mitochondrial structure was dominated by the baffle model, in which the larger surface of the inner membrane was accommodated within the space defined by the smaller outer membrane through the formation of broad folds called cristae that project into the mitochondrial matrix. In recent years, the baffle model has been displaced. Results from electron tomography of semithick sections have led to the crista junction model, in which the inner membrane is conceptually divided into two topological components—the inner boundary membrane that lies parallel and closely apposed to the outer membrane, and the cristae that are connected to the inner boundary membrane by tubular crista junctions of uniform diameter and variable length (1).

In some cell types, the tubular forms are thought to dominate. Aberrant inner membrane structures have been observed. For example, the inner membrane appears to form cubic phase structures in amoeba that are starved (2), while yeast mutants, lacking two nonessential subunits of the ATP synthase that are required to form enzyme dimers, result in abnormal inner membrane structures including formation of onion-skin structures (3). A deficiency of a dynamin-related protein, OPA1/mgm1p, required for inner membrane fusion, also produces aberrant inner membrane structures including individual vesicular matrix compartments that have been observed during apoptosis (4–6). Thus, specific inner membrane protein functions can exert a profound effect on membrane structure.

Tomograms of mitochondria in a HeLa cell and mouse embryonic fibroblast are shown in Fig. 1. The inner mitochondrial membrane is one complex surface comprised of the crista membrane and the inner boundary membrane; however, for clarity, the inner boundary membrane and each crista are displayed here in different colors. Each crista membrane contains a lamellar part and several tubular parts, and these tubes connect the lamella to the inner boundary membrane. In the course of this article, we deal only with morphology governed by structural motifs.

Theoretically, we pursue what can be termed the thermodynamic approach to account for the observed morphology of inner mitochondrial membranes. The lipid and protein molecules in these membranes are highly mobile (7) and the inner boundary membrane apposed to the outer membrane acts as a large reservoir of molecules for the crista membranes. Accordingly, it is reasonable to assume that the chemical potential of the molecules in the different parts of a crista are equal. This is equivalent to a statement that the shape of the crista membrane minimizes the free energy of these molecules. Fick's law on a sufficiently averaged timescale that is large compared with back-and-forth transitions has been amply verified for similar systems (8). Any difference in mean chemical potential, even for species represented by very few molecules, results, on the average, in the holding of Fick's law of transport. A corollary to this is that unless there are significant sinks and sources or active pumping of such species, they must, on the average, comprise a shape that has no chemical potential gradients—a shape of minimum free energy.

We recognize that many aspects of the morphology of the inner boundary membrane are likely due to the numerous proteins within and around the membrane. The presence and shape of such proteins can certainly affect the shape of the membrane much as the presence of a wire mesh (a scaffold) affects the shape of a soap bubble that forms on

Submitted April 2, 2010, and accepted for publication September 15, 2010.

*Correspondence: salamon@sdsu.edu

Editor: Reinhard Lipowsky.

© 2010 by the Biophysical Society

0006-3495/10/11/3244/11 $2.00

doi: 10.1016/j.bpj.2010.09.038

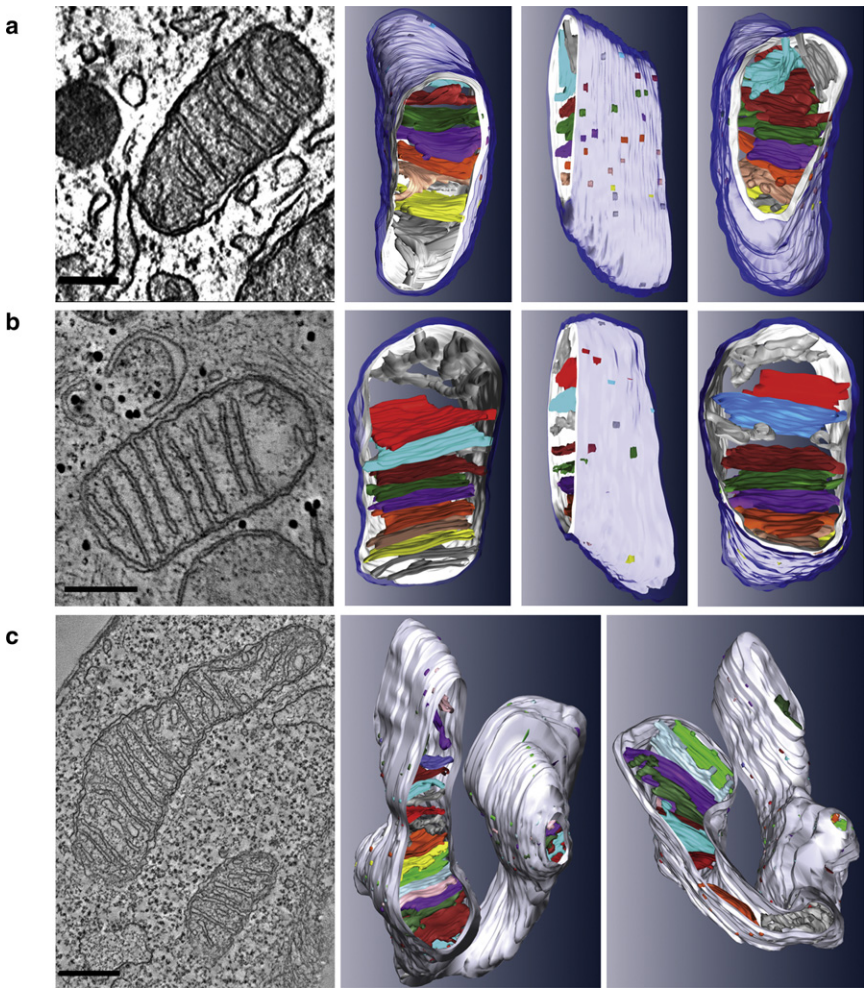

FIGURE 1 Electron tomography of the three mitochondrial volumes. These three volumes were used for measurements that were inserted in the free energy model to obtain thermodynamic parameters in each mitochondrion. (*Left*) Representative sections of constant z from the tomogram volumes. (*Right*) Three-dimensional models from volume segmentation and rendering. The successive views rotate about a vertical axis showing different parts of the three-dimensional models. The outer membrane is shown in translucent blue, the inner membrane in white and cristae in various colors. (*a* and *b*) Normal mitochondria from HeLa cells where dual-axis tomography enabled volume reconstruction of the mitochondria. (*c*) Normal mitochondrion from mouse embryonic fibroblast cells where dual-axis serial tomography on four successive sections enabled full volume reconstruction of the mitochondrion. Scale bar, 250 nm.

the wire mesh. In fact, several recent findings point to the possible presence of such a scaffold for the tubules (9–11). Nonetheless, the observed free and rapid movements of the lipids and proteins within these membranes (12) assures us that they distribute themselves in a way that minimizes their free energy subject to the constraints set by the scaffolding proteins in and around the membrane.

One striking feature of the observed crista shapes is their variability. Although there is an average shape that our measurements and calculations attempt to characterize, the magnitudes of the observed fluctuations around such an average shape are large. We conclude from this fact that the different crista shapes have free energies within k_BT of one another. This leads us to consider the entropy associated with such an ensemble of shapes and to the notion of shape entropy.

In two previous studies (13,14), we investigated how observed morphologies of restricted portions of the inner mitochondrial membranes can be used to infer thermodynamic information regarding typical configurations. Although a more first-principles approach (15) is of course preferable, it perforce assumes complete knowledge and understanding of the phenomena. As discussed above, cellular structures represent an intricate interplay between free energy-minimizing configurations and a backdrop of molecular agents and constraints. To untangle the complexities of cellular biophysics, our approach shows what we can expect without additional agents. Such considerations can lead to hypotheses concerning the presence and role of such additional agents. Our postulated tensile force on a crista arises in just such a fashion.

Our last study (13) focused on the radii of the tubules and their dependence on the osmotic pressure difference across the inner membrane by assuming that a tubular membrane makes up a thermodynamically stable structure that minimizes free energy. We showed that the observed tubular radii of ~10 nm correspond to a pressure that is ~0.2 atm lower in the inter membrane space, the compartment between the inner and outer membranes, than in the matrix space, the compartment enclosed by the inner membrane. Our previous model failed, however, to account for crucial features of the observed morphology. In particular, the

free energy of the tubular parts was higher than that of the lamellae. Hence, the tubes were predicted to be unstable to first order. Although some types of mitochondria have only vestigial tubes, many types show a composite structure incorporating both tubes and lamella.

In this work, we continue the line of reasoning regarding such coexistence by showing that a small tensile force can stabilize the tubular/lamellar structure to first order and calculate the magnitude of this force from observed morphologies. Tether pulling experiments (15,16) have observed that the force required beyond a vestigial tether is approximately independent of the length of the tether. We find that this is also the case for our model, and allows us to view the lamella-tubule coexistence as a phase equilibrium with the associated large fluctuations characteristic of phase transitions. Our analysis suggests that this phase transition is in large measure responsible for the varied shapes observed.

The article is organized as follows. In the next section, we introduce the simplified model of an average crista and derive the equations that minimize the energy for such model crista membrane. Then we discuss briefly how we obtain the geometrical parameters of our model crista membrane from measurements on the tomograms. A more detailed description can be found in the Supporting Material. From the model, we then deduce the values of thermodynamic properties implied by energy minimization: the tensile force required to stabilize the structure and predicted values of the pressure difference and surface tension of the crista membranes.

FREE ENERGY MODEL

The free energy of the inner mitochondrial membrane has a contribution from the inner boundary membrane and each of its crista membranes. In what follows we assume that the free energy is minimized by allowing variations in the size of the tubular and lamellar parts of the crista membranes, but that the number of cristae and the number of tubes in each crista remain fixed. Under that assumption, the shape of the entire inner membrane minimizes its free energy when each of the crista membranes minimizes its free energy. Hence we begin with the free energy for one crista membrane containing one laminar portion and N tubes as shown in Fig. 2 and study the conditions under which this free energy is minimized.

Although a biological membrane consists of a lipid bilayer ~5 nm thick with proteins extending beyond the bilayer on both sides, we treat the membrane as an infinitesimally thin sheet; our intent is to explore the implications of an analytic model incorporating the important effects in as simple a way as possible. One simplifying assumption is to take the topology of the membrane as fixed; we do not consider processes that involve connection or disconnection of different parts of the membrane. This enables us to ignore the Gaussian curvature term, because without changes in topology, the Gaussian curvature term in the energy is constant according to the Gauss-Bonnet theorem (17). Because our intent is to describe the observed morphologies in static micrographs, this is not a serious failure—provided we keep in mind that the reality may well be a rather dynamic movement among the possible shapes we characterize. We exploit this assumption of constant topology and take it a step further by neglecting the energy associated with crista junctions and in taking the spontaneous curvature of the surface to be zero. These last two assumptions introduce approximations that simplify the analysis presented at an acceptable level of cost in accuracy (see below).

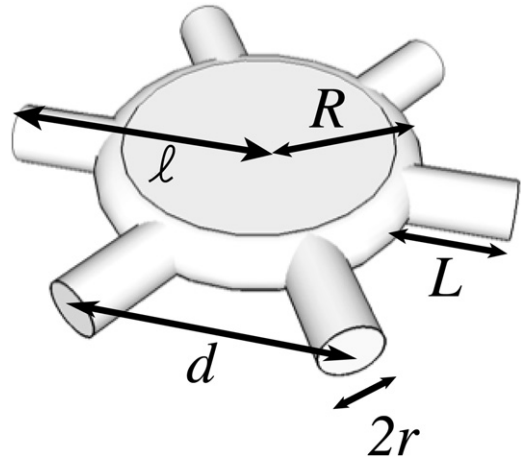

FIGURE 2 The simplified geometry of a crista membrane that is used to set up the equations of the free energy model. There are three sections of easily characterized geometry: 1), a flat lamellar section at the center, with radius R and thickness $2r$; 2), N tubular membranes, with radius r and length L; and 3), a semicylindrical membrane with radius r that wraps around the edge of the lamellae.

In this case, the energetic part of the free energy of one crista junction is described by a Helfrich free energy plus three additional energy terms describing the effect of surface tension, a radial pulling force and a pressure difference across the inner membrane, which separates the intermembrane region and the matrix space (18–20)

$$E = \frac{\kappa}{2}\int dA(C_1 + C_2 - C_0)^2 + \sigma\int dA - f_{tot}\ell - \Delta pV. \quad (1)$$

The first term is the Canham-Helfrich curvature energy for an infinitesimally thin fluid sheet, where κ is the bending elasticity, C_1 and C_2 are the principal curvatures, and C_0 is the spontaneous curvature. The integral is over the surface of the entire crista membrane. The second term is the energetic contribution due to the isotropic surface tension σ, whereby biomembranes can sustain a strain of a few percent in area before rupturing (21). The expression for the surface energy makes use of the fact that such energy per unit area, i.e., such surface tension, is the intensive parameter conjugate to surface area in the free energy. One

may alternatively regard σ as the Lagrange multiplier that serves to set the average area of the crista membrane (22). The term $f_{\mathrm{tot}}\ell$ represents the effect of the tensile force that pulls on the membrane. The force on each of the N tubular sections is $f = f_{\mathrm{tot}}/N$. The value ℓ is the distance from the center of the structure to the inner boundary membrane. It is equal to the sum of the radius R of flat circular lamellar membranes and the length L of the tubular parts (see Fig. 2).

One may regard f as the Lagrange multiplier that sets the average value of $\ell = R + L$. The last term comes from the difference between the pressure p_i in the intracristal space (inside the tubular parts) and the pressure p_m in the matrix space $\Delta p = p_{\mathrm{i}} - p_m < 0$. Note that the free energy in Eq. 1 only depends on the total volume and area of the membranes in the lamellar and tubular parts. As a result, a crista with tubules of several lengths distributed unevenly along the rim of the lamellar membrane has the same energy as a symmetric one, with a length equal to the average of the observed tube lengths. Hence, the configuration shown in Fig. 2 can be taken as the symmetric representative of a class of energetically equivalent structures. As seen below, this accounts for some of the observed variability in the tomograms. In particular, we note that this configuration represents N^{-1} degrees-of-freedom-worth of degeneracy, corresponding to varying the angles between the tubes.

The free energy of the crista is given by

$$F = E - TS, \tag{2}$$

where T is the ambient temperature and S is the entropy of the membrane. As we will see in the Discussion, the TS term has important implications for the resulting free-energy-minimizing shapes. For the present, we content ourselves by first examining the internal energy-minimizing shapes while neglecting the entropic term. This defines energetic basins in whose vicinity we find the states minimizing free energy.

To perform the integrals, we separate the crista membrane into three different portions:

1. A flat lamellar portion at the center, with radius R and thickness $2r$.
2. N tubular membranes, with radius r and length L.
3. A half-cylindrical shaped membrane with radius r that wraps around the edge of the lamellae.

This is an approximation made for simplicity. In particular, our model includes membrane at the junction between the tubes and the lamellae. Insofar as such area is constant, counting it or not counting it has no effect. This area does, however, depend on our parameter values (notably r). The total neglected area results in an overestimation of the total area in the curved portions of the membrane, areas 2 and 3, by, at most, 5%. Moreover, the shape of area 3 is actually a half-torus surrounding the lamella. We neglect the large radius R and count as though the periphery of the lamella were a half-cylinder, allowing us to combine this term with the term from the tubules. For a typical crista, neglecting the bending due to the large radius R introduces an error of $<0.5\%$ in our calculations.

Most importantly, our simple addition of the energies of these three portions neglects the contributions at the junctions where the tubes connect to the inner boundary membrane and the lamellae. In earlier studies (14), the junctions between tubules and the inner boundary membrane were found to resemble the bell of a trumpet. Moreover, the ratio of the radius of curvature of the flare of the trumpet and the radius of the tube r is assumed to be constant. Under these assumptions, the bending energy of the junction adds a constant term (independent of r and L) to the total bending energy. Hence, neglecting it will not alter Eq. 3 below. Modeling a junction as the bell of a trumpet will also introduce small changes ($\approx 0.1\%$) in the total surface area and volume of a typical crista. Neglecting the junction between the tubules and lamellar membrane will likewise introduce only small errors. The model breaks down for tube lengths below ~25 nm, though. Such short tubes are not present in the mitochondria shown in Fig. 1.

Next, we evaluate the contribution of each of the three portions to Eq. 1. Only portions 2 and 3 contribute to the bending energy. For a cylindrical membrane with radius r, $C_1 = 1/r$ and $C_2 = 0$. Assuming that there is no spontaneous curvature ($C_0 = 0$), the bending energy equals (21)

$$\frac{\kappa}{2}\int dA(C_1 + C_2 - C_0)^2 = \frac{\kappa}{2}\frac{A_c}{r^2},$$

where

$$A_c = 2\pi rLN + 2\pi^2 rR$$

is the total area of portions 2 and 3. The second term in Eq. 1 equals the surface tension times the area of all portions:

$$\sigma A = \sigma\left(2\pi R^2 + 2\pi rLN + 2\pi^2 rR\right).$$

The third term equals $fN(L+R)$ and the last term:

$$\Delta pV = \Delta p\left(2\pi rR^2 + \pi r^2 LN + \pi^2 r^2 R\right).$$

Taking the value of C_0 to be zero is an approximation that can have quite serious effects. We find that when $C_0 = 0.01\ \mathrm{nm}^{-1}$ the predicted value for the tensile forces f decreases by 25%. The value of Δp increases by 30% and that of σ decreases by 70%. The value of the bending modulus κ is also crucial for the calculation of these thermodynamic state variables, because they depend linearly on it. Unfortunately, the appropriate values of C_0 and κ for an inner mitochondrial membrane are not known. Hence, we assume that $C_0 = 0$ and $\kappa = 0.4\ 10^{-19}$ J—a typical value for a red blood cell or plasma membrane (21).

We proceed, keeping in mind that our assumptions for these membrane properties are the most serious of our

simplifications. Hence, the quantitative predictions made in this article should not be given too much credence. However, when the values of κ and C_0 for an inner mitochondrial membrane become available, it will be relatively easy to incorporate them into our model and obtain more accurate values for f, Δp, and σ. At this point, our goal is to show that the model makes reasonable predictions, if we assume reasonable values for C_0 and κ.

The energy is minimized by setting its derivatives with respect to the size of the tubules (r, L) and the size of the lamellae (R), equal to zero. This gives the following set of equations:

$$\begin{aligned}
&\frac{1}{r^2}(NL + \pi R) + \left(\frac{\Delta p}{\kappa}\right)(2NLr + 2R^2 + 2\pi rR) \\
&\qquad -\left(\frac{\sigma}{\kappa}\right)(2NL + 2\pi R) = 0, \\
&\frac{\pi}{r} - \left(\frac{f}{\kappa}\right) - \left(\frac{\Delta p}{\kappa}\right)\pi r^2 + \left(\frac{\sigma}{\kappa}\right)2\pi r = 0, \\
&\frac{\pi^2}{r} - \left(\frac{f}{\kappa}\right)N - \left(\frac{\Delta p}{\kappa}\right)(4\pi rR + \pi^2 r^2) \\
&\qquad + \left(\frac{\sigma}{\kappa}\right)(4\pi R + 2\pi^2 r) = 0.
\end{aligned} \tag{3}$$

Equation 1 has been successfully employed to analyze experiments in which tethers are drawn from large vesicles (15,16,23). When a point force is applied to the vesicle, a thin tether of constant radius forms and grows over time. The stress induces a shape transition, and as a result, the spherical vesicle coexists with a cylindrical tether. It can be shown that this state is a minimum of the energy in Eq. 1. The pressure difference goes as the inverse radius of the giant vesicle. Because this radius is of the order of a few microns, the pressure difference across the membrane can be neglected (15,19). The minimum of the energy in Eq. 1 for tether pulling from large vesicles can be obtained analytically. It follows that

$$r = \sqrt{\frac{\kappa}{2\sigma}}$$

and

$$f = \frac{2\pi\kappa}{r}.$$

Both the radius and force are constant during force-induced tether formation. In mitochondria, both the lamellar and tubular parts are at the scale of nanometers. Hence, the pressure difference is of importance, and the full set of expressions in Eq. 3 need to be solved numerically.

METHODS AND MEASUREMENTS

To solve Eq. 3 for the tensile force f, pressure difference Δp, and surface tension σ, we need values for the tube radius r, the average length of the tubes L, the number of tubes N, and the size of the lamellar section R. These data are obtained from tomograms such as those shown in Fig. 1. Clearly, none of the observed structures displays the ideal symmetric structure displayed in Fig. 2. Nevertheless, this geometry is motivated by the observations and represents an average crista membrane. The details on how we obtain measurements from the tomograms and analyze them to obtain the geometric parameters of our ideal structure can be found in the Supporting Material. Experimental protocol is described there as well.

In summary, values for r, L, d, and ℓ were obtained from the tomograms. From these values, $R = \ell - L$ and $N = 2\pi\ell$ Z/d were calculated. The geometrical parameters that we inserted in the model are listed in Table 1. We estimate that the error in a distance obtained from the tomograms is ~1.5 nm. Upon calculating the geometrical values, the error is sometimes reduced. For instance, the values for r are obtained

TABLE 1 Measured values and model predictions for Δp, σ, and f for all cristae

$\hat{r}$ (nm)	$\hat{R}$ (nm)	$\hat{L}$ (nm)	$\hat{\ell} = \hat{R} + \hat{L}$ (nm)	$\hat{N}$	Δp (atm)	σ (pN/nm)	f (pN)
HeLa mitochondrion 1							
9.9	154	32.2	186	7.6	−0.053	−0.023	12.9
10.2	175	36.7	211	15.5	−0.034	0.065	17.6
9.5	176	30.5	206	13.9	−0.044	0.041	16.9
9.5	205	36.4	241	19.7	−0.030	0.10	20.2
10.7	226	40.7	267	20.0	−0.019	0.089	18.4
11.7	194	46.4	240	18.8	−0.0076	0.12	19.7
10.2	106	42.8	149	8.8	−0.086	−0.033	13.1
HeLa mitochondrion 2							
10.5	168	36.7	205	15.1	−0.031	0.064	17.3
9.8	175	31.6	206	14.4	−0.040	0.047	17.0
9.8	206	35.3	241	20.5	−0.023	0.12	20.7
10.7	233	39.6	273	21.8	−0.014	0.11	19.6
11.7	195	45.4	240	18.1	−0.012	0.099	18.6
10.6	166	35.0	201	11.9	−0.039	0.018	14.4
9.9	164	33.6	197	11.7	−0.047	0.015	15.1
9.2	147	27.4	174	9.2	−0.061	−0.0081	14.8
Mouse embryonic fibroblast mitochondrion 3							
9.6	200	45.8	245	16.9	−0.042	0.057	17.8
9.7	199	51.8	251	17.4	−0.041	0.062	17.9
9.1	240	43.4	283	26.7	−0.017	0.17	24.2
9.2	253	55.5	308	30.4	−0.0011	0.23	27.1
10.3	256	48.4	305	25.9	−0.011	0.14	21.8
8.9	231	73.1	304	25.0	−0.038	0.14	22.7
9.1	235	54.5	289	23.5	−0.034	0.12	21.3
8.8	166	49.3	215	15.4	−0.069	0.048	18.7
8.8	145	60.5	205	9.21	−0.10	−0.041	14.4
8.9	228	37.9	266	26.6	−0.015	0.19	25.3
9.8	227	48.7	276	28.2	0.019	0.28	29.2
8.9	160	44.7	205	17.2	−0.052	0.10	21.0
9.3	224	35.8	260	24.3	−0.017	0.16	23.2
10.1	201	45.4	247	22.1	−0.0096	0.16	23.1
9.2	153	42.6	195	18.3	−0.025	0.17	23.9
8.8	158	35.6	193	17.7	−0.042	0.13	22.2
8.9	131	41.4	173	13.9	−0.072	0.062	19.4
8.1	134	37.0	171	18.6	−0.028	0.24	28.1
7.8	105	32.5	138	10.3	−0.14	−0.0086	18.4
10.1	107	37.6	145	11.2	−0.061	0.039	16.9

from averages over ~15 tubes and hence have an error of ~0.4 nm. The error in L is larger (≈ 1 nm) because the tubes are not perfectly straight. The error in the value of ℓ is quite large because, as discussed in the Supporting Material, a crista membrane has an elliptical instead of circular shape. As we will argue below, this is most likely due to dynamic fluctuations in the shape of the lamellar membrane.

RESULTS

Using the expressions in Eq. 3, the tensile force f_i, pressure difference Δp, and surface tension σ, have been calculated from the measured values for $\widehat{r}_i$, $\widehat{R}_i$, $\widehat{L}_i$, and $\widehat{N}_i$ for each of the 35 cristae studied. These results are shown in Table 1 as well. The bending modulus is taken to be $\kappa = 0.4\ 10^{-19}$ J, a typical value for a biological membrane (21). As can be seen from Eq. 3, the predicted values scale linearly with the bending modulus.

The tensile force is ~20 pN. It is of the same order of magnitude, but larger than the 5 pN typical for a molecular motor protein (15,21), suggesting that more than one motor protein is at work. The predicted pressure difference is negative, which is in agreement with the observation that the osmotic pressure in the matrix is larger than in the intermembrane space (14). It is significantly smaller than the 0.2 atm that we predicted in earlier work (13) in which tensile forces and surface tension were neglected. The actual value of the pressure drop across the inner mitochondrial membrane is not known, but we expect it to be significantly smaller than atmospheric pressure. The values for the surface tension obtained from our model seem reasonable as well: they are below 0.2 pN/nm, the value at which a typical biological membranes ruptures (21).

For these calculations, each crista was treated as a separate thermodynamic system. We expect, however, that Δp, representing the pressure difference across the inner membrane, would have the same value for all the cristae in equilibrium within the same mitochondrion. Similarly, the surface tension of the membrane σ should have the same value. Our view is that each crista within a given mitochondrion provides us, by way of the procedure described above, with an estimate of the true ambient Δp and σ characterizing the thermodynamic state of the mitochondrion. Our final estimates for Δp and σ (stated below) are computed as mean values accompanied by their standard errors. The actual source of error is manifold, and nearly impossible to evaluate reliably. It includes:

1. Fluctuations within the energetic basin.
2. Alterations from the biological state introduced in preparing the cells for electron microscopy.
3. Errors arising from the manner in which certain of the crista measurements are indirectly inferred from measurements of tomograms.

Given these caveats, the consistency of our measurements is encouraging.

Our results for the three mitochondria are as follows:

$$\begin{aligned}\Delta p &= -0.039 \pm 0.010 \text{ atm}\\ \sigma &= 0.051 \pm 0.023 \text{ pN/nm for mitochondrion 1,}\end{aligned}$$

$$\begin{aligned}\Delta p &= -0.033 \pm 0.006 \text{ atm}\\ \sigma &= 0.058 \pm 0.016 \text{ pN/nm for mitochondrion 2,}\end{aligned}$$

$$\begin{aligned}\Delta p &= -0.040 \pm 0.008 \text{ atm}\\ \sigma &= 0.122 \pm 0.018 \text{ pN/nm for mitochondrion 3.}\end{aligned}$$

Note that the Δp values are smaller by a factor of 5 than was predicted in the absence of the tensile force (13). To explore the robustness of our parameter values, we also estimated these parameters by finding the minimum distance configuration to our measurements in the space of configurations for the crista network with each crista having the same values for Δp and σ. The values were chosen to minimize the admittedly arbitrary distance

$$D = \sum_{i=1}^{m}\left[\frac{(\widehat{r}_i - r_i)^2}{r_i^2} + \frac{(\widehat{R}_i - R_i)^2}{R_i^2} + \frac{(\widehat{L}_i - L_i)^2}{L_i^2} + \frac{(\widehat{N}_i - N_i)^2}{N_i^2}\right]$$

between the measured values $\widehat{r}_i$, $\widehat{R}_i$, $\widehat{L}_i$,and $\widehat{N}_i$ and the configuration predicted from a shared value of Δp and σ. The sum is over the m different crista from the same mitochondrion. This method produced the following estimates:

$$\begin{aligned}\Delta p^* &= -0.030 \text{ atm and}\\ \sigma^* &= 0.068 \text{ pN/nm for mitochondrion 1,}\end{aligned}$$

$$\begin{aligned}\Delta p^* &= -0.029 \text{ atm and}\\ \sigma^* &= 0.065 \text{ pN/nm for mitochondrion 2,}\end{aligned}$$

$$\begin{aligned}\Delta p^* &= -0.025 \text{ atm and}\\ \sigma^* &= 0.126 \text{ pN/nm for mitochondrion 3.}\end{aligned}$$

Note that these results are within the standard errors of the first method while exhibiting a systematic overestimate relative to the first method. Nonetheless, the consistency is again encouraging.

Fig. 3 represents another kind of consistency check for our method. It compares the measured values of R, L, and N with some predicted values obtained by putting our estimates for the mitochondrial values of Δp and σ back into Eqs. 3. However, these three equations contain seven variables. Therefore, two additional values must be supplied (beyond the values of Δp and σ) before predictions can be made. We chose to use the measured values for r and ℓ for that purpose.

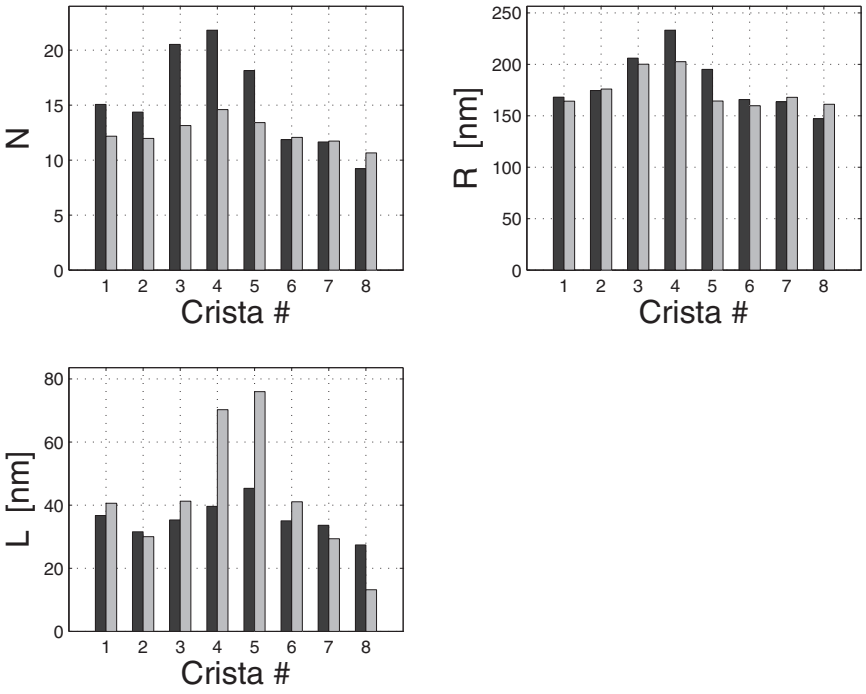

FIGURE 3 Comparison of predicted (*shaded*) and measured (*solid*) values of N, R, and L for the second mitochondria. The predicted values are obtained from the model for $\Delta p = -0.034$ atm, with $\sigma = 0.058$ pN/nm.

That the predicted tensile forces of ~20 pN are high compared to the typical force exerted by a molecular motor of 5 pN, could well be because of our assumed values for the bending modulus and spontaneous curvature. On the one hand, as we will speculate below, the proteins could be attached to the tubular part of the membrane and apply a tensile force through a scaffolding mechanism. Because multiple proteins are involved, the force exerted this way is expected to be higher than 5 pN.

We propose that this force is caused by the dynaminlike GTPase OPA1 that resides in the crista membrane. Olichon et al. (25) have shown that the loss of OPA1 perturbs the mitochondrial inner membrane structure. Without this enzyme and the hypothesized tensile force that it exerts, the crista membrane morphology is not stable. Knocking out OPA1 leads to abnormal cristae and the inner membrane fragments into individual vesicular matrix compartments (6). Moreover, knocking-out prohibitin results in absence of long isoforms of OPA1 and leads to the vesicular morphology (26). Furthermore, OPA1 is one of the proteins released during programmed cell death (apoptosis) (27), and its loss may be the cause of fragmentation of the inner membrane into vesicular matrix compartments observed during apoptosis (4).

DISCUSSION

The shape transition

The foregoing arguments have shown that adding a tensile force can stabilize the coexistence of tubules and lamellae in model crista. The intuition leading to these arguments came from thinking about the observed coexistence as the likely result of a shape transition under the influence of a tensile force. Such transitions are observed in other materials. For instance, if one pulls on one end of a polymer chain, it separates into a stretched and a coiled part, that coexist at a critical force (28). Likewise, a helical ribbon phase separates under the influence of a force into straight and helical parts (29). Such phase transition is also similar to what one sees in pulling tethers from vesicles (15,16,23). In all these studies, the force as a function of extension displays a plateau in the regime where both phases coexist. Extension is made possible by adjusting the fractions of the system in each of the two phases. Along such modes, the free energy change is zero, and this leads to large fluctuations and critical slowing-down.

Similarly, we expect the tubes and lamella of the inner mitochondrial membrane to represent two phases in equilibrium under the applied tensile force. The location of a crista membrane in a mitochondrion dictates its size ℓ and hence the relative distribution of the lipids over the tubes and the lamella. Increasing ℓ results in lengthening of tubes and shrinking of the lamella. To test this hypothesis, we plot the force f versus ℓ in Fig. 4. The curves are obtained from Eq. 3, using the Δp and σ-values of mitochondrion 2. As can be seen, the force reaches a constant value at high extensions. Such a constant force is also observed in the experiments that motivated our work (16,23). However, most of the experimental data do not fall on this plateau. Instead, the observed forces are slightly higher, and fall in the range where f depends on both ℓ and N. In this regime

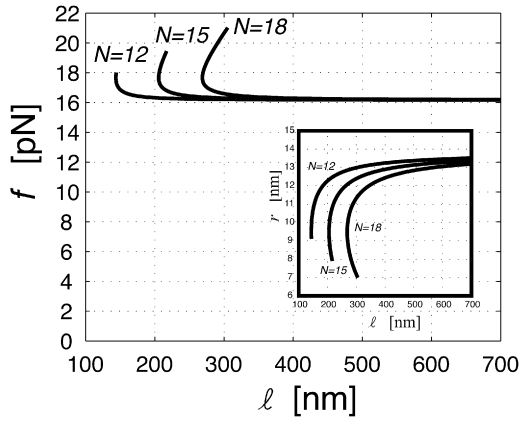

FIGURE 4 Tensile force f as a function of the size of a crista ℓ as predicted by our model for $\Delta p = -0.033$ atm and $\sigma = 0.058$ pN/nm. The constancy of f for larger ℓ values is a crucial part of our argument that we can view the tube-lamella coexistence as a phase equilibrium. Calculations are performed for $N = 12$, 15, and 18. The curves are parameterized by the tube length L. The upper branches correspond to smaller values of L than we have observed. (*Inset*) Tube radius r as a function of ℓ. Note that at low ℓ, r decreases, which causes f to increase.

the force has two values for a given ℓ that correspond to different values for L and R. The top branches in the figure have L values of <25 nm, which are not observed in our measurements. The increase in the force upon lowering ℓ in our model results from a decrease of the tube radius r. Unlike in the theory (15) for tethers pulled from giant vesicles, where

$$r = \sqrt{\frac{\kappa}{2\sigma}},$$

the radius r depends on ℓ in our model. This dependence is shown in the inset of Fig. 4. For given N, Δp, and σ, the dependence of the force f on r is dictated by the second line of Eq. 3. Hence, the deviation of the value of the force from a constant plateau value can be understood in terms of variations in tube radius.

Fluctuations

Results, above, showed that observed shapes of crista can consistently be associated with real crista shapes and the resulting model can be matched in a consistent way to the different cristae in the same mitochondrion sharing a pressure difference Δp and a surface tension σ. This association succeeds despite the obvious and varied shapes that real cristae assume, which are typically rather unlike our model depicted in Fig. 2. We look for the explanation of such variability by examining the fluctuations that we should expect to see in these structures.

An examination of the second derivative of the energy of one model crista in the three variables r_i, R_i, and L_i reveals an indefinite matrix with two stable directions and one unstable one. Let us examine the cone of instability for one of our examples. It turns out that this cone is very skinny; random perturbations of the stationary state at ($r = 10.2$ nm, $R = 174.5$ nm, and $L = 36.7$ nm) resulted in decreased free energy $<0.5\%$ of the time. As expected, the null direction that trades-off amount of tube for size of lamella is at the boundary of this very skinny cone (i.e., the second derivative of the energy along this coexistence direction vanishes).

It is generally true that the coexistence direction identically has $\Delta F = \Delta E - T\Delta S = 0$, and hence, the first and second derivatives of F along this direction must also vanish (30). In addition to the normal effects observed for tether pulling, there is an additional entropic effect as we move away from our symmetric configuration with stationary energy (see Fig. 2) by allowing some of our L values to differ from the minimum possible length. This corresponds to a fluctuation with $\Delta E = 0$ but $\Delta S > 0$, because it makes accessible several degrees of freedom that allow the lamella to move around, trading off L in one tube for L in another.

Beyond allowing such degrees of freedom to become active, the entropic contribution does not increase further—leaving us with an $N-1$ dimensional basin of minimum free energy that lies near the symmetric configuration of Fig. 2. As for any equilibrium system immersed in an environment at temperature T, the crista shape will explore variations with free energy changes ΔF on the order of k_BT. Given the magnitude of the tensile force f and the surface tension σ, fluctuations with an associated ΔE on the order of k_BT do not allow for significant changes in the total length of the tubes or in the total surface area of the crista. Equating $f\Delta\ell$ or $\sigma\Delta A$ to k_BT gives $\Delta\ell$ of ~1 nm and ΔA ~1 nm^2. It is only the two-phase coexistence along with the increase in shape entropy as we move away from symmetric configurations that make significant deviations possible, i.e., $\Delta\ell$ of ~15 nm and ΔA ~15 nm^2. The variability of the observed shapes also comes about in part from varying the angles around the lamella between the points of attachment for the tubes. As discussed in Free Energy Model, these degrees of freedom represent degeneracies of the energetically stationary state and explain the variability of the appearance of the crista.

To summarize, our tentative conclusions based on our model is that the energy-minimizing configurations at the given values of Δp, σ, and f do adequately represent approximate free energy minima, but are in fact only energetic stationary points—with nearby free energy minima that are stabilized by shape entropy terms, resulting in the varied structures observed. How the observed shapes match up with these entropic degrees of freedom is a question left for future effort.

Prolate spheroid shapes of mitochondria

The fact that healthy mitochondria exhibit elongated shapes (27) must be the work of proteins, because without them one

would expect the simple spherical shape displayed by, e.g., a soap bubble. The conventional wisdom (27) is that mitochondria attach to molecular motors that pull them along microtubules, thereby distorting their spherical shape. We hereby present an alternate mechanism in which the tensile forces exerted by the crista membranes on the outer membrane predicted by our model dictate the shape. As can be seen in Table 1 and Fig. 3, these tensile forces are slightly higher in the cristae that reside in the middle of a mitochondrion than in the crista closer to the edges. This is expected because the distortion from a spherical shape is larger in the middle.

The following rough estimate quantitatively supports this idea. The deformed mitochondrion has a higher energy than a spherical one. For mechanical equilibrium, the rate of change in energy with ℓ should be roughly equal to the sum of all tensile forces. Assuming that the area of the membrane is constant, the increase in the energy is due to an increase in volume and a change in bending energy. The second effect turns out to be negligible. Hence, we can write

$$\Delta p \frac{\partial V}{\partial \ell} = Nf, \tag{4}$$

where V is the volume between two crista membranes. It is related to the area A of the inner boundary membrane between these cristae by

$$V = \frac{A\ell}{2}.$$

Assuming that the area of the membrane is constant, it follows from Eq. 4 that

$$A = \frac{2Nf}{\Delta p}.$$

Let D be the distance between these crista, then

$$D = \frac{A}{2\pi\ell} = \frac{Nf}{\pi\ell\Delta p}. \tag{5}$$

Inserting the data from Table 1 for mitochondria 1, the predicted distance between two cristae equals 96 nm. This compares very well with the average measured value of 82 nm. Moreover, after treatment with etoposide (4), the shape becomes spherical. In this state, the cristae disappear as the matrix breaks up into vesicles.

CONCLUSIONS

This article takes an important step toward explaining the observed morphology of crista membranes in mitochondria. Although such morphology is highly varied, it often consists of coexisting tubes and lamella. Our previous attempt at understanding this coexistence failed (13); the lamellar portion seems always to have lower free energy. The study described here began with the realization that a tensile force such as the one used in tether pulling experiments, could in fact stabilize the coexistence we were trying to explain. We introduced a simple model incorporating such a tensile force and found its stationary states. The shapes of real cristae resembled these stationary states sufficiently closely that the parameters of the model could be identified, and consistent and reasonable values of the thermodynamic properties (Δp, σ, f) of the cristae observed could be calculated.

An examination of the second derivative of such internal energy showed there still exists a narrow cone of instability associated with the degree of freedom that interconverts lamellar and tubular portions. In this direction, however, we find that energetically degenerate states correspond to a many-dimensional space of crista-shape parameters and associate this degeneracy with a shape entropy that stabilizes such structures. An admittedly rough count shows the free energy minimum should lie some distance from the energy minimum. Note that the inference of such shape entropy is exactly in line with our overall method—to glean thermodynamic information from observed morphology. While we believe that it is possible to account for the distribution of tube lengths and deviations from circularity of the lamella from these considerations, we leave any attempt to do so for future efforts.

The tubular/lamellar crista structure in normal mitochondria is of functional importance. Healthy mitochondria contain one large matrix compartment in which products of mitochondrial DNA transcription and translation can reach all areas of the inner membrane. After treatment with etoposide, the tubular and lamellar crista components of many mitochondria disappear (4) with the formation of separate vesicular matrix compartments and impairment of mitochondrial function, which ultimately leads to cell death. During this process, the dynaminlike protein OPA1 is released (27). Hence, we speculate that this motor protein is responsible for the stabilizing tensile forces that are required in our model. Careful measurements show that OPA1 (the homologous protein in yeast is called mgm1p) is associated with the inner membrane and exposed to the intracristal space (31). It is speculated in Shaw and Nunnari (32) that OPA1/mgm1p stabilizes the crista membrane shape and plays an important role in mitochondrial compartment remodeling. How, to our knowledge, is not yet understood, but cartoons (32) often picture it as a spiral structure inducing a tubular curved shape. OPA1/mgm1p has an important function in other inner membrane remodeling events as well, most importantly those occurring during mitochondrial fusion (33).

We stress that this picture does not contradict our speculation that tensile forces stabilize the inner membrane shape. OPA1/mgm1p is a dynamin-related protein and the role of dynamin in remodeling the shape of membranes is well documented (10,11). It self-assembles into rings and spirals and wraps around budding vesicles where it plays a key role in membrane fission. In a recent study, Roux et al. (9) added dynamin during a tether pulling experiment. They find that

dynamin polymerizes around the tube and thereby acts along the tube direction. Hence, to model the role of dynamin, they add an additional tensile force to the thermodynamic model, which is employed to explain tether-pulling experiments. Their experimental results agree with those obtained by minimizing the thermodynamic free energy obtained in our approach. Interestingly, they find that the tensile polymerization force in their experiment is ~18 pN, which is substantially larger than the typical force exerted by a molecular motor protein (5 pN). We envision that the mechanism by which OPA1 exerts a tensile force could be very similar to this one.

We realize that, in addition to such a scaffolding mechanism, there are others by which proteins or lipids could impose curvature to a biological membrane (34). We think that it is unlikely that any of these play a critical role in stabilizing the tubular components of the inner mitochondrial membrane. For instance, it is known that helical insertions in one leaflet of the membrane or the presence of asymmetric integral membrane proteins can cause a strong spontaneous curvature. However, such a mechanism cannot explain the coexistence of tubular and lamellar parts in the crista membrane. Cytoskeleton remodeling cannot be involved, as the inner mitochondrial membrane is not exposed to the cytoplasm. Finally, we have shown in earlier work (13) that lipid composition can only play a minor role in shaping the crista membrane. However, membrane-associated proteins, such as OPA1/mgm1p, most likely play a crucial role through the mechanism described above. The thought that dynamin-like proteins shape membranes and regulate remodeling processes by exerting tensile forces is an intriguing one. If this is indeed the case, it might enable us to construct novel theories to explain membrane curvature and its crucial role for the proper function of cellular processes.

SUPPORTING MATERIAL

Explanation of experimental protocol, and two figures, are available at http://www.biophysj.org/biophysj/supplemental/S0006-3495(10)01186-0.

We thank Sander Pronk, Karl Heinz Hoffmann, and Udo Seifert for useful discussions and suggestions, Rob Phillips for carefully reading and criticizing the manuscript, and Steven Barlow and Sogand Taheri of San Diego State University electron microscopy facility for assistance with preparation of samples for electron microscopy. We acknowledge M. McCaffery, Z. Song, and D. C. Chan for the mouse embryonic fibroblasts, M. Sun for the HeLa cells, and the National Center for Microscopy and Imaging Research at the University of California, San Diego for advice, software, and computer support.

This project was supported by a Blasker Science and Technology grant from the San Diego Foundation to T.G.F.

REFERENCES

1. Frey, T. G., and C. A. Mannella. 2000. The internal structure of mitochondria. *Trends Biochem. Sci.* 25:319–324.
2. Deng, Y., M. Marko, …, C. A. Mannella. 1999. Cubic membrane structure in amoeba (*Chaos carolinensis*) mitochondria determined by electron microscopic tomography. *J. Struct. Biol.* 127:231–239.
3. Paumard, P., J. Vaillier, …, J. Velours. 2002. The ATP synthase is involved in generating mitochondrial cristae morphology. *EMBO J.* 21:221–230.
4. Sun, M. G., J. Williams, …, T. G. Frey. 2007. Correlated three-dimensional light and electron microscopy reveals transformation of mitochondria during apoptosis. *Nat. Cell Biol.* 9:1057–1065.
5. Griparic, L., N. N. van der Wel, …, A. M. van der Bliek. 2004. Loss of the intermembrane space protein Mgm1/OPA1 induces swelling and localized constrictions along the lengths of mitochondria. *J. Biol. Chem.* 279:18792–18798.
6. Song, Z., M. Ghochani, …, D. C. Chan. 2009. Mitofusins and OPA1 mediate sequential steps in mitochondrial membrane fusion. *Mol. Biol. Cell.* 20:3525–3532.
7. Hackenbrock, C. R., B. Chazotte, and S. S. Gupte. 1986. The random collision model and a critical assessment of diffusion and collision in mitochondrial electron transport. *J. Bioenerg. Biomembr.* 18:331–368.
8. Stock, G., K. Ghosh, and K. A. Dill. 2008. Maximum Caliber: a variational approach applied to two-state dynamics. *J. Chem. Phys.* 128:194102.
9. Roux, A., G. Koster, …, P. Bassereau. 2010. Membrane curvature controls dynamin polymerization. *Proc. Natl. Acad. Sci. USA.* 107:4141–4146.
10. Hinshaw, J. E. 2000. Dynamin and its role in membrane fission. *Annu. Rev. Cell Dev. Biol.* 16:483–519.
11. Sweitzer, S. M., and J. E. Hinshaw. 1998. Dynamin undergoes a GTP-dependent conformational change causing vesiculation. *Cell.* 93:1021–1029.
12. Gupte, S., E. S. Wu, …, C. R. Hackenbrock. 1984. Relationship between lateral diffusion, collision frequency, and electron transfer of mitochondrial inner membrane oxidation-reduction components. *Proc. Natl. Acad. Sci. USA.* 81:2606–2610.
13. Ponnuswamy, A., J. Nulton, …, A. R. Baljon. 2005. Modeling tubular shapes in the inner mitochondrial membrane. *Phys. Biol.* 2:73–79.
14. Renken, C., G. Siragusa, …, T. G. Frey. 2002. A thermodynamic model describing the nature of the crista junction: a structural motif in the mitochondrion. *J. Struct. Biol.* 138:137–144.
15. Phillips, R., J. Kondev, and J. Theriot. 2008. Physical Biology of the Cell. Taylor & Francis Group, London, UK.
16. Brochard-Wyart, F., N. Borghi, …, P. Nassoy. 2006. Hydrodynamic narrowing of tubes extruded from cells. *Proc. Natl. Acad. Sci. USA.* 103:7660–7663.
17. Millman, R. S., and G. D. Parkas. 1977. Elements of Differential Geometry. Prentice-Hall, New York.
18. Bozic, B., S. Svetina, …, R. E. Waugh. 1992. Role of lamellar membrane structure in tether formation from bilayer vesicles. *Biophys. J.* 61:963–973.
19. Seifert, U. 1997. Configurations of fluid membranes and vesicles. *Adv. Phys.* 46:13–137.
20. Wortis, M., J. H. Yao, and M. Wortis. 1996. Stability of cylindrical vesicles under axial tension. *Phys. Rev. E Stat. Phys. Plasmas Fluids Relat. Interdiscip. Topics.* 54:5463–5468.
21. Boal, D. 2001. Mechanics of the Cell. Cambridge University Press, Cambridge, UK.
22. Brown, F. L. H. 2008. Elastic modeling of biomembranes and lipid bilayers. *Annu. Rev. Phys. Chem.* 59:685–712.
23. Upadhyaya, A., and M. P. Sheetz. 2004. Tension in tubulovesicular networks of Golgi and endoplasmic reticulum membranes. *Biophys. J.* 86:2923–2928.
24. Reference deleted in proof.
25. Olichon, A., L. Baricault, …, G. Lenaers. 2002. Loss of OPA1 perturbates the mitochondrial inner membrane structure and integrity. *J. Biol. Chem.* 278:7743–7746.

26. Merkwirth, C., S. Dargazanli, …, T. Langer. 2008. Prohibitins control cell proliferation and apoptosis by regulating OPA1-dependent cristae morphogenesis in mitochondria. *Genes Dev.* 22:476–488.

27. Arnoult, D., A. Grodet, …, C. Blackstone. 2005. Release of OPA1 during apoptosis participates in the rapid and complete release of cytochrome *c* and subsequent mitochondrial fragmentation. *J. Biol. Chem.* 280:35742–35750.

28. Halperin, A., and E. B. Zhulina. 1991. On the deformation behavior of collapsed polymers. *Eur. Phys. Lett.* 15:417–421.

29. Smith, B., Y. V. Zastavker, and G. B. Benedek. 2001. Tension-induced straightening transition of self-assembled helical ribbons. *Phys. Rev. Lett.* 87:278101.

30. Weinhold, F. 1976. Metric geometry of equilibrium thermodynamics. V. Aspects of heterogeneous equilibrium. *J. Chem. Phys.* 65:559.

31. Wong, E. D., J. A. Wagner, …, J. Nunnari. 2000. The dynamin-related GTPase, Mgm1p, is an intermembrane space protein required for maintenance of fusion competent mitochondria. *J. Cell Biol.* 151:341–352.

32. Shaw, J. M., and J. Nunnari. 2002. Mitochondrial dynamics and division in budding yeast. *Trends Cell Biol.* 12:178–184.

33. Meeusen, S. L., and J. Nunnari. 2005. How mitochondria fuse. *Curr. Opin. Cell Biol.* 17:389–394.

34. McMahon, H. T., and J. L. Gallop. 2005. Membrane curvature and mechanisms of dynamic cell membrane remodeling. *Nature.* 438:590–596.